Available online at www.sciencedirect.com
ScienceDirect
Trans. Nonferrous Met. Soc. China 25(2015) 803−810
Transactions of Nonferrous Metals Society of China
www.tnmsc.cn

Microstructure and high temperature oxidation resistance of Si−Y co-deposition coatings prepared on TiAl alloy by pack cementation process

Yong-quan LI[1,2], Fa-qin XIE[2], Xiang-qing WU[2]

1. School of Materials Science and Engineering, Beifang University of Nationalities, Yinchuan 750021, China;
2. School of Aeronautics, Northwestern Polytechnical University, Xi'an 710072, China

Received 31 March 2014; accepted 10 December 2014

Abstract: In order to improve the high temperature oxidation resistance of TiAl alloy, Y modified silicide coatings were prepared by pack cementation process at 1030, 1080 and 1130 °C, respectively, for 5 h. The microstructures, phase constitutions and oxidation behavior of these coatings were studied. The results show that the coating prepared by co-depositing Si−Y at 1080 °C for 5 h has a multiple layer structure: a superficial zone consisting of Al-rich $(Ti,Nb)_5Si_4$ and $(Ti,Nb)_5Si_3$, an out layer consisting of $(Ti,Nb)Si_2$, a middle layer consisting of $(Ti,Nb)_5Si_4$ and $(Ti,Nb)_5Si_3$, and a γ-TiAl inner layer. Co-deposition temperature imposes strong influences on the coating structure. The coating prepared by Si−Y co-depositing at 1080 °C for 5 h shows relatively good oxidation resistance at 1000 °C in air, and the oxidation rate constant of the coating is about two orders of magnitude lower than that of the bare TiAl alloy.
Key words: TiAl alloy; Si−Y co-deposition coating; microstructure; high temperature oxidation resistance; pack cementation process

1 Introduction

In recent years, Ti−Al based intermetallics have received significant attention, since they possess low density, high specific strength and low cost compared to currently used nickel-based super alloys [1−3]. It is estimated that, with the use of TiAl alloy in aero-engine, potential component weight savings of over 50% can be achieved over conventional super alloys [4]. However, the high temperature oxidation resistance of TiAl alloys is relatively poor because they can hardly form a continuous Al_2O_3 scale, but the non-protective TiO_2 and Al_2O_3 mixed scale [5]. This becomes a "notable" problem that impacts the performances of TiAl alloys [6]. Thus, a protective coating is necessary for the high-temperature applications of TiAl alloy.

Hence, a number of techniques including ion implantation, plasma spray and sputtering deposition have been studied in the past decades to improve the oxidation resistance of TiAl alloy [7]. Among these techniques, the pack cementation, which is a combination of high volume, low capital and operating cost and applicable for a wide range of shapes and sizes, has been widely accepted and used in a broad range of applications to enhance the surface properties of nickel-based superalloys and steel components with great success [8], but that was seldom reported on TiAl alloy.

Due to the formation of a protective SiO_2 scale with sufficient low growth rate at high temperature, silicide coatings were extensively employed to improve the surface properties of nickel and Ti components [9]. However, the brittleness of silicide coatings always leads to cracking and spalling. Therefore, modified elements such as Al, B, Zr and Y. have been employed to develop the silicide coatings. Among these elements, Y has been reported to be beneficial in reducing the grain size and improving the ductility of the coatings [10−13].

In this work, Si−Y co-deposition coatings were prepared on a TiAl alloy by halide activated pack cementation (HAPC) technique. The structures and the phase constituents of the Si−Y co-deposition coatings were studied. The oxidation behaviors of both TiAl substrates and coatings at 1000 °C were also investigated.

2 Experimental

The TiAl alloy used in this work was supplied by the State Key Laboratory of Solidification Processing of

Foundation item: Project (2014JZ012) supported by the Natural Science Program for Basic Research in Key Areas of Shaanxi Province, China
Corresponding author: Fa-qin XIE; Tel/Fax: +86-29-88494371; E-mail: fqxie@nwpu.edu.cn
DOI: 10.1016/S1003-6326(15)63666-4

China with a nominal composition of Ti−35Al−9Nb (mole fraction, %). Samples used in experiments were cut into 10 mm×10 mm×3 mm by electro-discharge machining and ground with 1000 grit SiC paper, and then ultrasonically cleaned in an acetone bath just before coating preparation.

The Si−Y co-deposition coatings were prepared in an electric tube furnace with the pack mixtures composing of $15Si−2Y_2O_3−8NaF−75Al_2O_3$ (mass fraction, %). While the Si and Y_2O_3 powders were used as donor sources, the NaF powder was used as activator and the Al_2O_3 powder was used as filler. Before the experiments, each kind of the powders was weighed according to the ratio and then mixed up by tumbling in a ball mill for 4 h. The coating preparation process was the same as what has been reported in Ref. [14]. In detail, specimens to be coated were firstly buried in the pack powders in an alumina crucible, which were then sealed with an Al_2O_3-based silica sol binder. According to the results of our previous study [14], the co-deposition temperature was selected as 1030, 1080 and 1130 °C, respectively. The furnace was heated to these temperatures at a rate of 15 °C/min. After holding at the co-deposition temperature for 5 h, the specimens were furnace cooled to room temperature.

The oxidation behaviors of both TiAl alloy and coating specimens were examined at 1000 °C isothermally in static air in an electric furnace. The coating specimen was placed in an alumina crucible, so that the total mass change including spalled oxides could be obtained. Prior to the oxidation test, the crucible was heated at 1200 °C until no mass change was observed. The mass changes of the specimens were monitored by intermittent weight measurement and weighed in an electronic balance with an accuracy of 0.1 mg. The specimens were rapidly taken out of the furnace to cool at room temperature and then placed back into the furnace after a weight measurement.

X-ray diffraction analysis (XRD, Panalytical X'Pert PRO), was employed to identify the phases of both coating and oxidized specimens. Their cross-sectional microstructure and chemical composition of the constituent phases were analyzed by a scanning electron microscope (SEM, JSM−6360LV) equipped with an energy dispersive spectroscopy (EDS).

3 Results and discussion

3.1 Coating structure

Figure 1 presents the surface and cross-sectional backscatter electron (BSE) images of the Si−Y co-deposition coatings prepared at 1080 °C for 5 h. As can be seen in Fig. 1(a), the coating had a compact surface free of micro-cracking and spalling. The cross-sectional BSE images of the coating (Fig. 1(b)) revealed that the coating with a total thickness of about 41 μm, possessed five distinctive layers.

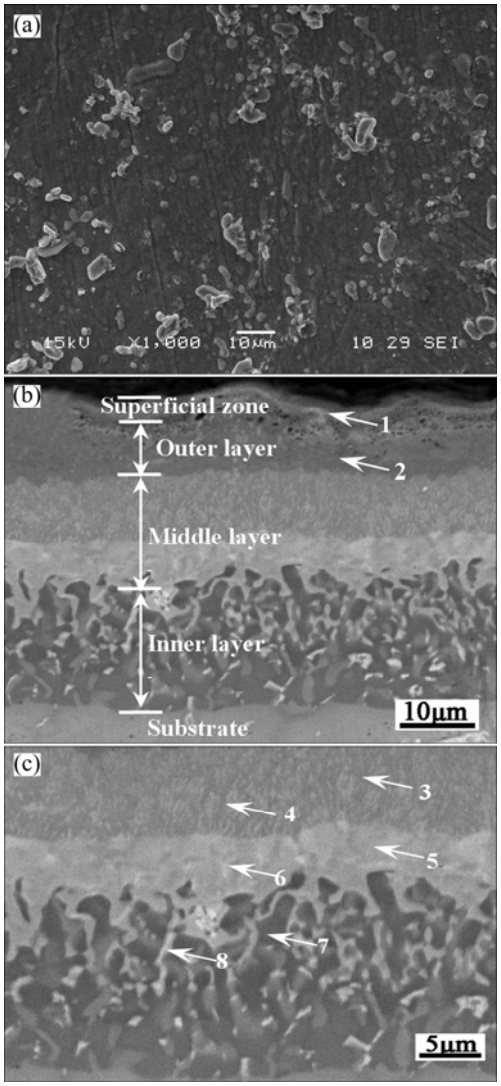

Fig. 1 BSE images of Si−Y co-deposited coating prepared at 1080 °C for 5 h: (a) Surface morphology; (b) Cross-sectional BSE image; (c) Enlarged BSE images of middle layer and inner layer

Figure 2 shows the XRD patterns conducted respectively on the surface, outer layer, middle layer and inner layer of the coating, and Table 1 presents the EDS analysis results of the typical constituent phases in each layer. It can be seen that the superficial zone of the coating was about 3 μm in thickness, possessing a composition of 6.49Al−37.60Si−48.33Ti−6.97Nb−0.61Y (mole fraction, %) (Table 1, site 1). According to the binary Ti−Si phase diagram [15], this superficial zone could be composed of Al-rich $(Ti,Nb)_5Si_4$ and $(Ti,Nb)_5Si_3$ phases, which were also confirmed by the XRD pattern conducted on the surface of the coating (Fig. 2(a)). It should be emphasized that Ti and Nb could

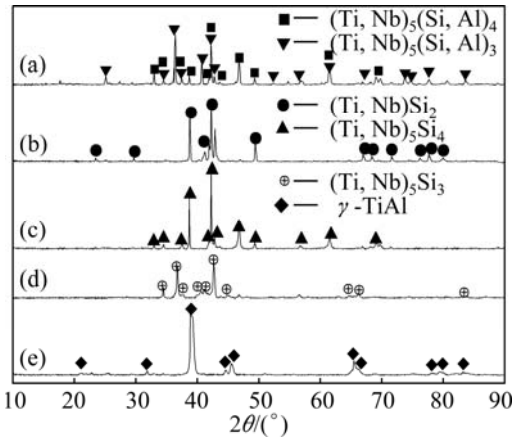

Fig. 2 XRD patterns of original surface (a) of Si−Y co-deposition coating prepared at 1080 °C for 5 h and surfaces after coating being stripped off about 5 μm (outer layer) (b), 11 μm (outer portion of middle layer) (c), 20 μm (lower portion of middle layer) (d) and 30 μm (inner layer) (e), respectively

Table 1 Chemical compositions determined by EDS analysis of sites marked by arrows with numbers 1−8 in Fig. 1 (molar fraction, %)

Site	Mole fraction/%				
	Al	Si	Ti	Nb	Y
1	6.49	37.60	48.33	6.97	0.61
2	−	63.21	31.59	4.57	0.63
3	−	41.77	52.60	5.05	0.58
4	−	44.60	48.30	6.64	0.46
5	−	35.85	58.14	5.62	0.39
6	−	35.55	54.23	9.77	0.45
7	42.68	2.78	46.65	7.89	−
8	36.93	10.32	43.09	9.66	−

be observed in the pack mixtures adjacent to the surface of the coating. As Nb and Ti were not the deposition elements containing in the pack mixtures, the appearance of Ti and Nb in the pack could be an evidence of outward diffusion mechanism and/or reactions between the substrate and the vapor phases in the pack. Thus, it is reasonable to deduce that the formation of the coating in superficial zone could be resulted from two possible mechanisms: 1) both outward diffusion of Ti and Nb from the base alloy and the inward diffusion of Si in the pack; 2) Ti and Nb in the coating reacted with the activator (NaF) or other vapor species such as SiF_x (x=1−4) and AlF_y (y=1−3) to produce the Ti and Nb containing vapor species in the pack. However, further experiments should be carried out to confirm whether these two explanations are correct.

Beneath the superficial zone, there existed an out layer with a thickness of about 8 μm, EDS analysis revealed that it had a composition of 63.21Si−31.59Ti−4.57Nb−0.63Y (mole fraction, %) (Table 1, site 2). Together with the binary Ti−Si phase diagram [15] and XRD analysis results (Fig. 3(b)), this outer layer was determined to be $(Ti,Nb)Si_2$.

As shown in Fig. 1(c), the middle layer was about 15 μm thick and had a double-layer structure, consisting of gray matrix (Fig. 1, site 3) in its outer portion and light-gray matrix (Fig. 1, site 5) in its lower portion. EDS analysis proved that the gray matrix (Table 1, site 3) had a composition of 41.77Si−52.60Ti−5.05Nb−0.58Y (mole fraction, %), while the light-gray matrix (Table 1, site 5) had a composition of 35.85Si−58.14Ti−5.62Nb− 0.39Y (mole fraction, %). Together with the binary Ti−Si phase diagram [15] and XRD analysis results (Figs. 2(c) and (d)), the gray matrix was determined to be $(Ti,Nb)_5Si_4$, and the light-gray matrix was determined to be $(Ti,Nb)_5Si_3$. Moreover, it was easily found that some bright tissues were present throughout the middle layer. From the EDS analysis results (Table 1, sites 4 and 6)), it was obvious that these bright tissues were Nb-rich phases.

The inner layer was about 15 μm thick and showed a discontinuous morphology, characterized by dark gray matrix and white noodle-like tissues. EDS analyses demonstrated that the dark gray matrix (Fig. 1, site 7) had a composition of 42.68Al−2.78Si−46.65Ti−7.89Nb (molar fraction, %), while the noodle-like tissues (Fig. 1, site 8) had a composition of 36.93Al−10.32Si−43.09Ti−9.66Nb (mole fraction, %). Together with the binary Ti−Al phase diagram [16] and XRD analysis results (Fig. 2(e)), both the dark gray matrix and the noodle-like tissues in the inner layer were supposed to be composed of γ-TiAl. However, it should be noted that the content of Si in the white noodle-like tissues (10.32%, molar fraction) was higher, but the content of Al (36.93%) was much lower when compared with those in the dark matrix, which suggested that the white noodle-like tissues were Si-rich γ-TiAl. Additionally, it can also be seen that the inner layer of the coating possessed higher Al content when compared with the base alloy, because the solid solubility of Al in silicide coating was lower than that in the Ti−Al based alloy [17]. In this case, it is reasonable to deduce that the higher content of Al in the inner layer could be resulted from the inward diffusion of Si, which pushed Al element from the coating to the substrate gradually.

3.2 Effects of temperature on coating structure

Figure 3 presents the cross-sectional BSE images and element content profiles of the Si−Y co-deposition coatings prepared at respectively 1030 °C and 1130 °C for 5 h. It is obvious that the co-deposition temperature imposed strong influences on the coating structure. As

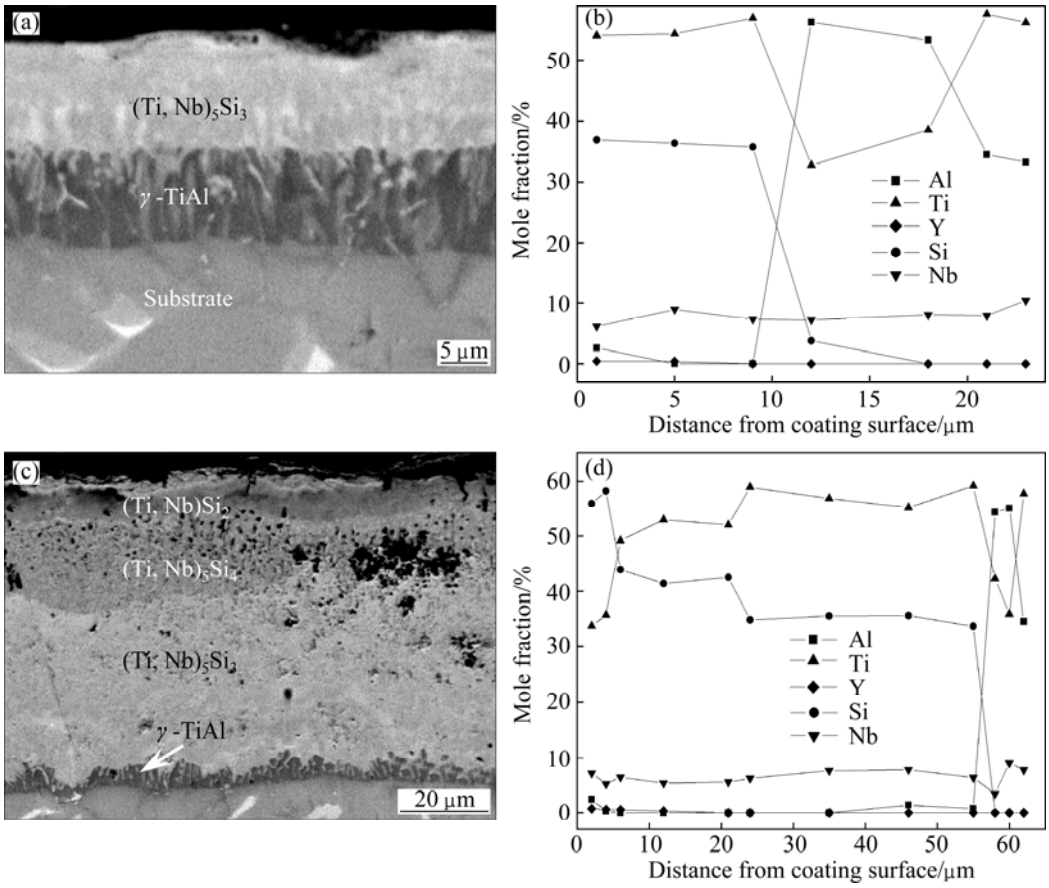

Fig. 3 Cross-sectional BSE images and element content profiles of Si−Y co-deposition coatings prepared at 1030 °C (a, b) and 1130 °C (c, d) for 5 h

can be seen from Fig. 3(a), the coating prepared at 1030 °C was only about 20 μm thick, mainly consisting of two layers. XRD pattern conducted on the surface of the coating (Fig. 4) revealed that the outer layer of the coating was mainly composed of $(Ti,Nb)_5Si_3$ phase, which was also confirmed by EDS analyses (Fig. 3(b)). The inner layer was mainly composed of gray matrix and noodle-like tissues. EDS analysis results suggested that both gray matrix and noodle-like tissues were γ-TiAl, which were similar to the inner layer of the coating prepared at 1080 °C for 5 h. The lower content of Si in the coating could be harmful to the oxidation resistance of the coating, because the formation of a continuous SiO_2 scale requires a content of Si exceeding 40% in the coating.

However, the thickness of the coating increased up to about 60 μm with increasing the co-deposition temperature to 1130 °C, and the coating structure was also very different from that of the coating prepared at 1030 °C, as can be seen in Fig. 3(c). Both EDS analysis (Fig. 3(d)) results and XRD pattern conducted on the surface of the coating (Fig. 4) revealed that the structure of the coating prepared at 1130 °C was similar to that of the coating prepared at 1080 °C, consisting of a

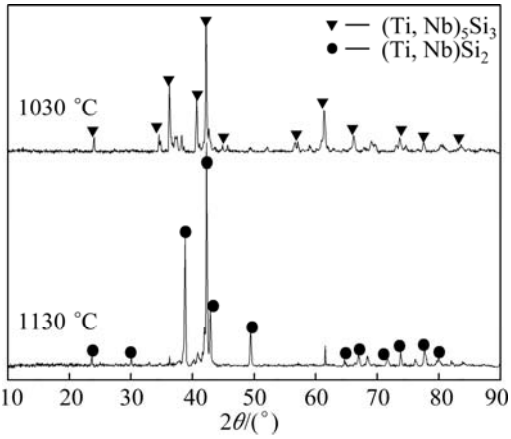

Fig. 4 XRD patterns conducted on surfaces of Si−Y co-deposition coatings prepared at respectively 1030 °C and 1130 °C for 5 h

$(Ti,Nb)Si_2$ out layer, a middle layer with $(Ti,Nb)_5Si_4$ in its upper portion and $(Ti,Nb)_5Si_3$ in its lower portion, and a γ-TiAl inner layer. It should be noted that numerous holes could be observed in the middle layer of the coating, as shown in Fig. 3(c). These holes could be caused by the outward diffusion of Ti and Nb during the coating formation process, which could produce

vacancies in the coating.

Based on the structure of the co-deposition coatings prepared at respectively 1030, 1080 and 1130 °C, it was reasonable to deduce that the phase formation and transformation mechanisms in the coatings might be explained as follows: with the uninterrupted inward diffusion of Si from the pack to the substrate, $(Ti,Nb)_5Si_3$ formed firstly by the reaction of 5Ti+5Nb+3Si→ $(Ti,Nb)_5Si_3$, which had the lowest formation enthalpy (−588.86 kJ/mol), followed by the reactions of $(Ti,Nb)_5Si_3$+Si→$(Ti,Nb)_5Si_4$ and $(Ti,Nb)_5Si_4$+Si→ $(Ti,Nb)Si_2$, which would drive Al element from coating surface to the substrate and form the γ-TiAl inner layer, as a result of the lower solid solubility of Al in Si silicides than those in the Ti−Al base alloy [18]. Moreover, $(Ti,Nb)_5Si_3$ was regarded as the front interface of the reactive diffusion of Si during the coating formation process, and remained in the front of $(Ti,Nb)_5Si_4$ layer finally. These reactions would consume Si element and lead to the deficiency of Si atoms in the pack at the last stage of the co-deposition process. And also, it is considered that the solid state diffusion coefficient of the elements in the coating can be described as an exponential relationship with the deposition temperature. Therefore, the increased co-deposition temperature would course of increase both inward diffusion of Si and outward diffusion of Ti and Nb in the coating. As a result, vacancies produced by the outward diffused Ti and Nb cannot be refilled by Si, and gradually accumulated to form holes in the coating prepared at high temperature (1130 °C). These holes would offer an easy path for the inward diffusion of O during the oxidation process, which could be harmful to the oxidation resistance of the coating.

3.3 Oxidation behavior of selected coatings at 1000 °C

3.3.1 Oxidation kinetics

The Si−Y co-deposition coating prepared at 1080 °C for 5 h was selected for oxidation test. Figure 5 presents the oxidation kinetics of both Si−Y co-deposition coating and TiAl based alloy at 1000 °C. It could be found that the mass gain of the coatings was nearly linear to a square root of oxidation time, which suggested that the oxidation kinetic of the coating followed a parabolic law. This parabolic law introduced that the oxidation process of the Si−Y co-deposition coating was controlled by diffusion. Considering that the parabolic equation was described as $y^2=k_p t$, where y is the mass gain, t is the oxidation time and k_p is the parabolic rate constant of oxidation, the parabolic rate constants for the oxidation of the bare alloy and the Si−Y co-deposition coating were respectively 4.54 and 4.04×10^{-2}. It can be seen that the oxidation rate constant of the Si−Y co-deposition coating was lower than that of the bare TiAl alloy by about two orders of magnitude. Obviously, the Si−Y co-deposition coating possesses much better oxidation resistance than that of the bare alloy at 1000 °C.

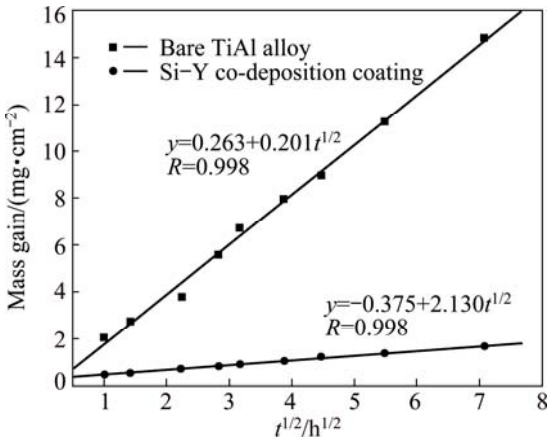

Fig. 5 Comparison of oxidation kinetics of Si−Y co-deposition coating and TiAl based alloy at 1000 °C

3.3.2 Oxide scale morphologies

Figure 6 shows the cross-sectional BSE image and surface XRD pattern of the TiAl based alloy after oxidation at 1000 °C for 10 h (when the oxidation time was longer than 10 h, the oxide scale formed on the TiAl based alloy flaked off during the cooling process). The elemental contents characterized by EDS analysis in the typical area of the scale (sites 9−12) are given in Table 2. It can be seen that the oxidation scale is basically composed of two typical phases: the light-gray phase (sites 9 and 11) with a typical composition of 61.26O−33.06Ti−5.67Al, and the dark phase (site 10) with a typical composition of mainly composed of 40.99O−32.29Al−26.72Ti. Together with the XRD patterns shown in Fig. 6(b), the light-gray phase was determined to be TiO_2, and dark phase could be a mixture of TiO_2 and Al_2O_3. Beneath the scale, there exists a thin white zone (site 12). EDS analysis results demonstrated that the white zone had a composition of 29.22Al−47.72Ti−23.06Nb, suggesting that it was Nb-rich TiAl.

From the above discussion, it was obvious that the scale formed on the based alloy was mainly composed of TiO_2, with little Al_2O_3, though the content of Al in the base alloy was as high as 35%. These results were in agreement with RAKOWSKI et al [19], who studied the oxidation behavior of γ-TiAl at 1000 °C. It has also been reported that only if the content of Al in the binary Ti−Al alloys exceeds 60%, a stable Al_2O_3 scale can form on the alloy [20]. As the diffusion rate of O in the TiO_2 is larger than that in Al_2O_3, the mixed TiO_2 and Al_2O_3 scale could be less protective compared with continuous Al_2O_3 scale and/or SiO_2 scale.

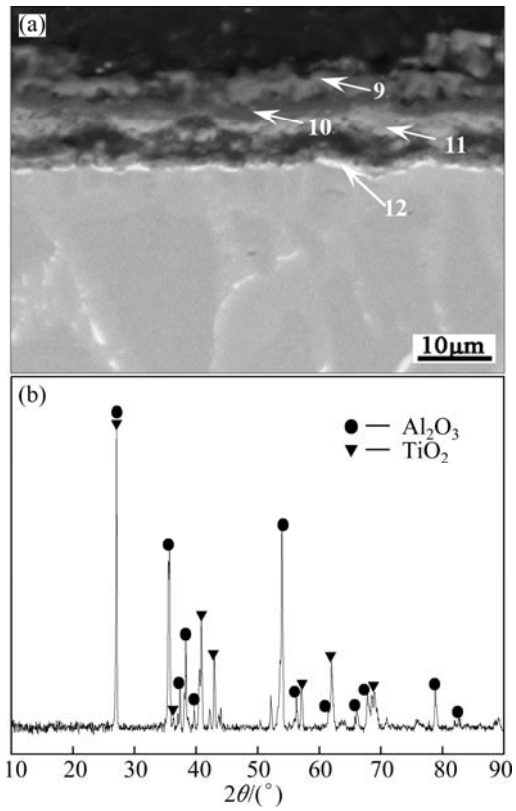

Fig. 6 Cross-sectional BSE image (a) and XRD pattern (b) of surface of TiAl alloy after oxidation at 1000 °C for 10 h

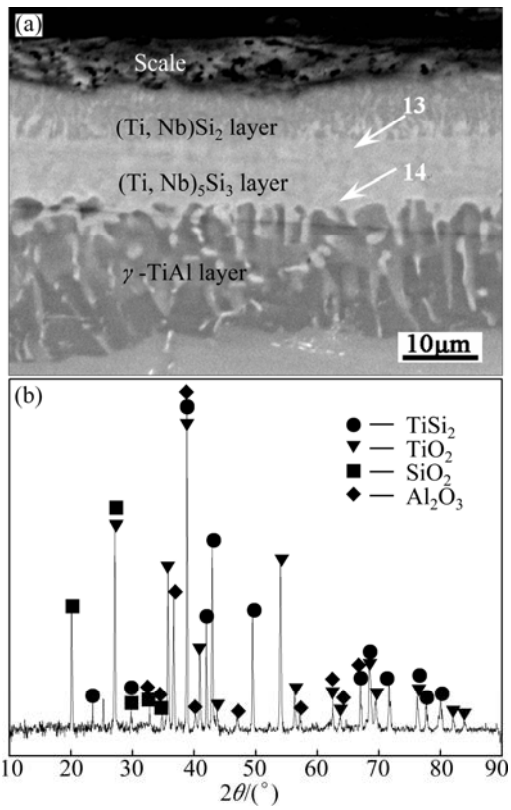

Fig. 7 Cross-sectional BSE image (a) and XRD pattern (b) of surface of Si−Y co-deposition coatings after oxidation at 1000 °C for 10 h

Table 2 Chemical compositions determined by EDS analysis of sites marked by arrows with numbers 9−12 in Fig. 6(a)

Site	O	Al	Ti	Si	Nb	Y
9	61.26	5.67	33.06	−	−	−
10	40.99	32.29	26.72	−	−	−
11	57.04	0.59	37.76	−	4.61	−
12	−	29.22	47.72	−	23.06	−

Figure 7 shows the cross-sectional BSE image and surface XRD pattern of the Si−Y co-deposition coating after oxidation at 1000 °C for 10 h. It can be seen that the scale was about 5 μm thick, with numerous pores formed on the surface of the coating. EDS analysis results revealed that it had a composition of 65.23O−1.33Al−29.73Ti−3.14Si−0.57Nb. According to the XRD pattern (Fig. 7(b)), the scale was determined to be TiO_2, with low contents of Al_2O_3 and SiO_2. This was consistent with QIAO et al [21] who have studied the oxidation behavior of Ti_5Si_3, and their results revealed that the formation of TiO_2 was prior to SiO_2 in the scale. Beneath the scale, $(Ti,Nb)Si_2$ layer remained. However, compared with the coating before oxidation (Fig. 2(b)), it can be found that the thickness of the $(Ti,Nb)Si_2$ outer layer decreased to about 6 μm while that of the $(Ti,Nb)_5Si_3$ middle layer increased from 6 μm to 12 μm. And also, the original $(Ti,Nb)_5Si_4$ middle layer disappeared after oxidation at 1000 °C for 10 h, as revealed by EDS analysis results (sites 13 and 14 in Fig. 7(a)), and this could be mainly resulted from the transformation of $(Ti,Nb)_5Si_4 \rightarrow (Ti,Nb)_5Si_3+Si$.

Figure 8 presents the cross-sectional BSE images and XRD pattern conducted on the surface of the Si−Y co-deposition coating after oxidation at 1000 °C for 50 h. It can be seen that a dense scale with a thickness of about 10 μm formed on the coating. Beneath the scale, numerous holes could be observed in the middle portion of the remained coating. Moreover, it was easily found that the thickness of the remained $(Ti,Nb)_5Si_3$ middle layer increased from 11 μm to 25 μm, while that of the γ-TiAl inner layer decreased to 7 μm. This could be resulted from both outward diffusion of Si and Ti to form oxides and the continuous inward diffusion of Si in the coating during the oxidation process.

From the enlarged cross-sectional BSE image (Fig. 8(b)), it can also be seen that the scale had two layers: the outer layer was mainly composed of dark matrix and light-gray tissues, and the inner layer was mainly composed of gray phase. EDS analyses revealed that the dark matrix in the outer layer had a composition of 74.78O−1.50Al−17.83Si−4.41Ti−0.88Nb−0.60Y and

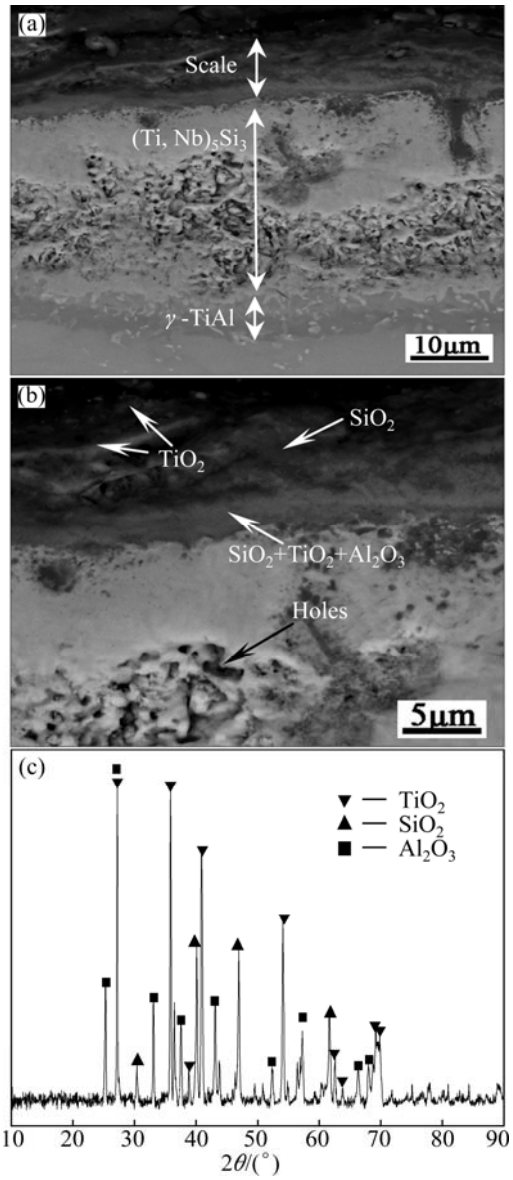

Fig. 8 Cross-sectional BSE images (a, b) and XRD pattern (c) of surface of Si−Y co-deposition coating after oxidation at 1000 °C for 50 h

the light-gray tissues had a composition of 67.88O−32.12Ti, which indicated that the dark matrix and light-gray tissues in the outer layer were respectively SiO_2 and TiO_2. While the gray phase of inner layer possessed a composition of 62.28O−5.88Al−21.65Si−8.87Ti−0.72Nb, which indicated that it was composed of a mixture of SiO_2, TiO_2 and Al_2O_3. These results from EDS were also confirmed by the XRD pattern conducted on the surface of the coating, as shown in Fig. 8(c).

From the above discussion, it could be found that the SiO_2 was the dominate phase in the scale. As the diffusion rate of O in SiO_2 was much lower than that in TiO_2, lower content of TiO_2 in the scale could be beneficial in promoting the oxidation resistance of the coating. Moreover, it should be noted that Y was mainly detected in SiO_2 phase, the incorporation of Y in the external scale improved the sintering characteristics and plasticity of the oxides, which reduced the stress in the scale, and therefore the scale could adhere to the coating firmly after oxidation at 1000 °C for 50 h [22]. Moreover, TIAN et al [23] have reported that the existence of Y in the scale could suppress the outward diffusion of Ti during the oxidation process, which subsequently resulted in a lower oxidation rate compared to the TiAl based alloy.

4 Conclusions

1) The Si−Y co-deposition coatings prepared at 1080 °C for 5 h had a multiple layer structure, consisting of an Al-rich $(Ti,Nb)_5Si_4$ and $(Ti,Nb)_5Si_3$ superficial zone, a $(Ti,Nb)Si_2$ out layer, a $(Ti,Nb)_5Si_4$ and $(Ti,Nb)_5Si_3$ middle layer, and an γ-TiAl inner layer.

2) Co-deposition temperature imposed strong influences on the coating structure. The coating prepared at 1030 °C for 5 h mainly consisted of a $(Ti,Nb)_5Si_3$ outer layer and γ-TiAl inner layer. The coating prepared at 1130 °C had similar coating structure with that prepared at 1080 °C for the same holding time of 5 h, except for numerous hole formed in its middle layer.

3) The Si−Y co-deposition coating prepared at 1080 °C for 5 h possessed relatively good isothermal oxidation resistance at 1000 °C in air. After oxidation, a dense scale consisted of SiO_2, Al_2O_3 and TiO_2 formed on the coating. The growth of the scale obeyed a parabolic kinetics, and the oxidation rate constant of the coating was lower than that of the bare TiAl alloy by about two orders of magnitude.

References

[1] TANG Z L, WANG F H, WU W T. Effect of Al_2O_3 and enamel coatings on 900 °C oxidation and hot corrosion behaviors of gamma-TiAl [J]. Materials Science and Engineering A, 2000, 276(1): 70−75.

[2] MA X X, HE Y D, LIN J P, WANG D R. Effect of a magnetron sputtered (Al_2O_3−Y_2O_3)/(Pt−Au) laminated coating on hot corrosion resistance of 8Nb−TiAl alloy [J]. Surface and Coatings Technology, 2012, 206(10): 2690−2697.

[3] WANG Q M, MYKHAULONKA R, FLORES R A, LEYENS C, KIM K H. Improving the high-temperature oxidation resistance of a β-γ TiAl alloy by a Cr_2AlC coating [J]. Corrosion Science, 2010, 52(11): 3793−3802.

[4] XIANG Z D, ROSE S R, BURNELL J S. Co-deposition of aluminide and silicide coatings on γ-TiAl by pack cementation process [J]. Journal of Materials Science, 2003, 38(1): 19−28.

[5] BECKER S, RAHMEL A, SCHORR M. Mechanism of isothermal oxidation of the intermetallic TiAl and of TiAl alloys [J]. Oxidation of Metals, 1992, 38(5−6): 425−464.

[6] ZHAO W Y, XU B W, MA Y, GONG S K. Inter-phase selective corrosion of γ-TiAl alloy in molten salt environment at high

temperature [J]. Progress in Natural Science: Materials International, 2011, 21(4): 322−329.
[7] WU Xiang-qing, XIE Fa-qin, HU Zong-chun, WANG Li. Effects of additives on corrosion and wear resistance of micro-arc oxidation coatings on TiAl alloy [J]. Transactions Nonferrous Metals Society of China, 2010, 20(6): 1032−1036.
[8] LIN N M, GUO J W, XIE F Q, ZOU J J, TIAN W, YAO X F. Comparison of surface fractal dimensions of chromizing coating and P110 steel for corrosion resistance estimation [J]. Applied Surface Science, 2014, 311: 330−338.
[9] RIVIERE J P, PICHON L, DROUET M. Silicon based coatings deposited by dynamic ion mixing for oxidation protection of a Ti6242 alloy [J]. Surface and Coatings Technology, 2007, 201(19): 8343−8347.
[10] QI T, GUO X P. Microstructure and high temperature oxidation resistance of Si−Y_2O_3 co-deposition coatings prepared on Nb-silicide-based ultrahigh temperature alloy by pack cementation process [J]. Journal of Inorganic Materials, 2009, 6: 1219−1225.
[11] BIANCO R, RAPP R A, JACOBSON N S. Volatile species in halide-activated diffusion coating packs [J]. Oxidation of Metals, 1992, 38(1−2): 33−43.
[12] ZHANG P, GUO X P. Y and Al modified silicide coatings on an Nb−Ti−Si based ultrahigh temperature alloy prepared by pack cementation process [J]. Surface and Coatings Technology, 2011, 206(2): 446−454.
[13] QI Fu-gng, ZHANG Ding-fen, ZHANG Xiao-hua, PAN Fu-sheng. Effect of Y addition on microstructure and mechanical properties of Mg−Zn−Mn alloy [J]. Transactions Nonferrous Metals Society of China 2014, 24(5): 1352−1364.
[14] LI Y Q, XIE F Q, WU X Q, LI X. Effects of Y_2O_3 on the microstructures and wear resistance of Si−Al−Y co-deposition coatings prepared on Ti−Al alloy by pack cementation technique [J]. Applied Surface Science, 2013, 287: 30−36.
[15] RAMOS A S, NUNES C A, COELHO G C. On the peritectoid Ti_3Si formation in Ti−Si alloys [J]. Materials Characterization, 2006, 56(2): 107−111.
[16] KATTNER U R, HANDWERKER C A. Calculation of phase equilibria in candidate solder alloys [J]. Zeitschrift fur Metallkunde, 2001, 92(7): 740−746.
[17] ZHAO J C. Reliability of the diffusion-multiple approach for phase diagram mapping [J]. Journal of Materials Science, 2004, 39(12): 3913−3925.
[18] ZELENITSAS K, TSAKIROPOULOOS P. Study of the role of Al and Cr additions in the microstructure of Nb−Ti−Si in situ composites [J]. Intermetallics, 2005, 13(10): 1079−1095.
[19] RAKOWSKI J M, PETTIT F S, MEIER G H. The effect of nitrogen on the oxidation of γ-TiAl [J]. Scripta Metallurgica at Materialia, 1995, 33(6): 997−1003.
[20] COCKERAM B V, RAPP R A. Oxidation-resistant boron-and germanium-doped silicide coatings for refractory metals at high temperature [J]. Materials Science and Engineering A, 1995, 192−193: 980−986.
[21] QIAO Y Q, GUO X P. Formation of Cr-modified silicide coatings on a Ti−Nb−Si based ultrahigh-temperature alloy by pack cementation process [J]. Applied Surface Science, 2010, 256(24): 7462−7471.
[22] ZHANG P, GUO X P. A comparative study of two kinds of Y and Al modified silicide coatings on an Nb−Ti−Si based alloy prepared by pack cementation technique [J]. Corrosion Science, 2011, 53: 4291−4299.
[23] TIAN X D, GUO X P. Structure and oxidation behavior of Si−Y co-deposition coatings on an Nb silicide based ultrahigh temperature alloy prepared by pack cementation technique [J]. Surface and Coatings Technology, 2009, 204(3): 313−318.

包渗工艺制备 TiAl 合金表面 Si−Y 共渗层的组织和抗高温氧化性能

李涌泉[1,2]，谢发勤[2]，吴向清[2]

1. 北方民族大学 材料科学与工程学院，银川 750021；
2. 西北工业大学 航空学院，西安 710072

摘　要：通过在 1030，1080 和 1130 °C 下扩散共渗 5 h 在 TiAl 合金表面制备 Y 改性的硅化物渗层，分析共渗层的显微组织及相组成，并对其高温抗氧化性能进行研究。结果表明：共渗温度对共渗层的组织有显著影响，在 1080 °C 共渗 5 h 所制备的共渗层由外向内依次为富 Al 的$(Ti,Nb)_5Si_4$和$(Ti,Nb)_5Si_3$表层、$(Ti,Nb)Si_2$外层、$(Ti,Nb)_5Si_4$和$(Ti,Nb)_5Si_3$中间层及 γ-TiAl 内层。1080 °C 共渗 5 h 制备的共渗层在 1000 °C 下具有良好的抗高温氧化性能，且渗层的氧化速率常数较基体的约降低了 2 个数量级。

关键词：TiAl 合金；Si−Y 共渗层；显微组织；抗高温氧化性能；包渗工艺

(Edited by Yun-bin HE)